Real-time Monitoring of Trehalose Crystallization using Quantum Cascade Laser Microscopy and 2D-COS

Yesenia M. Acevedo Rivera[a], Michael Meléndez[a] and Belinda Pastrana-Ríos[a*]

[a]Protein Dynamic Solutions, Inc. Wakefield, MA 01880, USA.

Correspondence to Belinda Pastrana-Ríos: Protein Dynamic Solutions, Inc. 9 Audubon Road, Wakefield MA 01880; E-mail: belinda@pdsbio.com.

Abstract

Molecular detail of the trehalose crystallization process was obtained during thermal perturbation through real-time monitoring using a Quantum Cascade Laser (QCL) microscope and 2D correlation spectroscopy. We were able to separate QCL IR spectral data based on the hyperspectral images acquired into key segments that defined the crystallization events: **(1)** trehalose in solution or the pre-transition phase, **(2)** nucleation and crystallization transition and **(3)** the crystal growth phase. Furthermore, the hyperspectral images allowed for the determination of the region of interest (ROI) allowing for the selection of QCL IR spectral data directly associated with the crystallization process. This approach allowed for the distinction of different types of intermolecular Hydrogen bonding interactions and dynamics involving α,α-trehalose with its aqueous environment, the dihydrate and between trehalose molecules. To our knowledge this is the first time that a real-time description of the molecular events that lead to trehalose crystallization have been described.

Keywords
trehalose; dehydration; crystallization; quantum cascade laser infrared microscope; hyperspectral imaging; two-dimensional infrared correlation spectroscopy; thermal perturbation

Funding:
The work presented herein is due to the funding support from the National Science Foundation (NSF) SBIR PII Award 1632420 (BPR).

1. Introduction

Trehalose is a naturally occurring disaccharide known for its ability to protect biomolecules from stress conditions such as high and low temperatures, chemical oxidation, osmotic shock, and dehydration [1]. One of its most relevant applications is the effective stabilization of proteins during freeze–thaw, heat–cooling and dehydration–rehydration cycles [2]. To date, protein stability is one of the biggest challenges faced by the biopharmaceutical industry as the number of therapeutic protein products are being developed world wide [3]. The protective effects of trehalose has made it a frequently used excipient in biotherapeutic formulations working both as a stabilizer of proteins in solution and a lyoprotectant during lyophilization [4, 5]. In solution, trehalose increases the surface tension of water promoting the hydration of the protein [4]. Whereas during lyophilization,

trehalose substitutes the water molecules and interacts directly with the dried protein through Hydrogen bonding [6, 7]. Trehalose also serves as a cryoprotectant throughout product preservation by disrupting the water structure decreasing the formation ice crystals [8]. This suggests that the molecular interactions between trehalose and water molecules may explain the bioprotective effect of trehalose [9]. However, understanding the molecular processes presented above remains elusive.

The chemical structure of trehalose confers the molecule the chemical and physical properties that distinguishes it from other bioprotective disaccharides such as sucrose and maltose. Trehalose is thermally and chemically stable, non-reducing and two glucose containing disaccharide linked by an α(1,1)-glycosidic bond (**Fig. 1**). This glycosidic bond protects the sugar from acid and α-glucosidase hydrolysis, keeps the disaccharide in a closed-chain form, and prevents covalent binding to protein residues and other biomolecules [1]. Trehalose has a single intra-molecular Hydrogen bond and when in solution, it forms multiple Hydrogen bonds with water making it a highly soluble molecule. However, unlike other disaccharides at high concentrations, pure trehalose undergoes a phenomenon where it assumes a conformation in solution analogous to the trehalose dihydrate crystalline state [10, 11]. The delimiting concentration for this high concentrated state is approximately 60% (w/v) [12].

To our knowledge, the present study describes for the first time, the molecular process of trehalose crystallization using hyperspectral images acquired through Quantum Cascade Laser Infrared Microscopy (QCL IRM) in real-time. The transformative events of α,α-trehalose in solution, nucleation crystallization and crystal growth are remarkable in combination with the molecular understanding through 2D IR correlation spectroscopy focused on in-phase simultaneous events that occurred with an unprecedented level of detail.

2. Materials and Methods

2.1. Trehalose preparation

Highly pure commercially available α,α-trehalose dihydrate was purchased from Affymetrix, Inc. (Cleveland, Ohio) and dissolved in deionized H_2O (resistivity of 18 megohm) to a concentration of 65% (w/v).

2.2. Quantum Cascade Laser Infrared Microscopy

A 1 µL aliquot of the 65% (w/v) trehalose solution was added to a pre-defined well of a custom milled CaF_2 slide and covered with a fully polished crystal to make up the slide cell. The slide cell was then placed in a heated accessory with accurate (± 0.5 °C) thermal control and Hyperspectral Images (HSI's) were acquired within the temperature range of 24.0 - 60.0 °C with 2 °C intervals and 4 min equilibration periods using ProteinMentor™, a quantum cascade laser microscope from Protein Dynamic Solutions, Inc. (Wakefield, MA).

2.3. Hyperspectral image acquisition

Three quantum cascade lasers are the source of enhanced signal to noise ratios (SNR) allowing for a linear response microbolometer focal plane array (480 x 480 pixels) detector to be used. For spatial resolution, a low magnification objective (4x) with a numerical aperture of 0.3 NA with a 2 x 2 mm^2 field of view (FOV) providing a pixel size of 4.25 x 4.25 μm spatial resolution. The HSI's are comprised of 223,000 QCL IR spectra and were collected at 4 cm^{-1} resolution within the spectral region of 1750 - 1500 cm^{-1}. To prevent coherence effects due to QCL fluctuations, the background was collected at each set temperature once thermal equilibrium (4 min) was achieved.

2.4. 2D IR Correlation Spectroscopy

This technique builds upon the infrared spectroscopy high selectivity and sensitivity by adding four main advantages: **(1)** enhancing the resolution of highly overlapped bands within the spectral region of interest, **(2)** establishing the peak assignments through peak correlations, **(3)** separating peak phase changes observed into two separate plots and **(4)** describing the molecular behavior of biomolecules during perturbation, while in their aqueous environment. Furthermore, peak width changes can also be observed as part of the dynamic spectral features that are observed due to the perturbation. 2D IR correlation spectroscopy was developed by Noda [14-16].

Briefly, the QCL IRM spectral data set was subject to the subtraction of the initial α,α-trehalose spectrum at 24 °C within the spectral region of 1760 - 1200 cm^{-1} to generate difference spectra. A correlation function was applied to the difference spectral data set using the Hilbert-Noda transformation matrix [16] to obtain the synchronous and asynchronous plots. The analysis spreads the acquired QCL IRM difference spectra in two dimensions, thus enhancing the spectral resolution. The ***synchronous plot*** contains the simultaneous in phase peak intensity changes that occurred due to the perturbation. A unique feature of *synchronous plot,* are *auto peaks* located on the diagonal which represent the extent of intensity change during the thermal perturbation (24 – 60 °C). This plot also contains *cross peaks* that define the correlation between peaks that change within the spectral region of interest. Unlike the previous plot the ***asynchronous plot*** only contains *cross peaks* that change in intensity out-of-phase from one another. Herein we have focused the evaluation of the simultaneous spectral changes that were observed using the synchronous plot. Since, trehalose is comprised of two identical cyclic structures the synchronous plot would contain those changes that were concurrent in both rings, thus allowing for a consistent approach to the analysis. The peak width and intensities changes observed could be directly associated to the stage of crystallization. The peak width for the O-H bending vibrational modes within trehalose would be indicative of the extent, type and strength of Hydrogen bonding interactions due to its effect on the electron density for the O-H group [17]. Moreover, the correlations established provided a molecular level of understanding during the real-time monitoring of the crystallization process of trehalose.

The spectral data was not manipulated, and only baseline correction was performed using the Correlation Dynamics™ software, from Protein Dynamics Solution, Inc. (Wakefield, MA).

3. Results and discussion

3.1. Band Assignments

Trehalose QCL IRM spectra were analyzed within the spectral region of 1760-1200 cm^{-1} and a temperature range of 24 – 60 ºC containing H_2O water bending vibration, OH deformation and scissoring methylene modes within the pyranose rings (Table 1). Allowing for an in-depth analysis of crystallization process of trehalose.

For the band assignments we used the correlation between the cross peaks and the auto peaks within the synchronous plot, allowing us to distinguish between the aqueous associated modes within 1760 – 1500 cm^{-1} from the vibrational modes of the α,α-trehalose dissacharide within 1500 – 1200 cm^{-1} (Fig. 2). The spreading of the spectral data into two dimensions provides enhanced spectral resolution, and allows for assertive band assignments for the entire temperature range 24 – 60 ºC also summarized in Table 1: H_2O bending vibrations (1683, 1651, 1643, 1638, 1631 and 1613 cm^{-1}) are consistent with varying Hydrogen bonding strength due to the increase in temperature and the water molecules within the trehalose crystal. However, the peak at 1631 cm^{-1} corresponds to H_2O bending vibration involving the shell of water that is Hydrogen bonding to the Trehalose OH groups. For trehalose: *first pyranose ring* the ***pre-transition phase (24 - 36ºC)*** included carbon 2 δ(O-H) at 1416 cm^{-1}, carbon 3 δ(O-H) at 1320 cm^{-1} and carbon 6 δ(O-H) at 1237 cm^{-1}. No auto peaks were observed for the second pyranose ring. During the ***nucleation-crystallization phase (40 - 44 ºC)*** bending vibrations δ(O-H) for carbons 4, 3 and 6 were observed at 1422, 1256 and 1231 cm^{-1}, respectively were observed. For the *second pyranose ring* the bending vibrations δ(O-H) at 1435, 1377 and 1314 cm^{-1} were assigned to carbons 3', 6' and 4', respectively. For the ***crystal growth phase (52 - 60 ºC)*** the bending vibrations δ(O-H) for carbons 4, 3 and 6 at 1458, 1332 and 1274 cm^{-1}, respectively. Also, observed was the scissoring mode of the methylene group $\delta(CH_2)$ at 1453 cm^{-1}. For the *second pyranose ring* carbon 4' δ(O-H) at 1312 cm^{-1}, carbon 3' δ(O-H) at 1236 cm^{-1}, and carbon 6' the CH_2OH group has the δ(O-H) at 1250 cm^{-1} and the scissoring mode of the methylene group $\delta(CH_2)$ at 1443 cm^{-1} was observed. These assignments are in good agreement with the available crystal structure, DFT calculations, and other works [18-20].

3.2. Hyperspectral images and 2D IR Correlation Spectroscopy

The QCL IR spectra are representative of the region of interest (ROI) within the hyperspectral image (HSI) where the trehalose crystal was observed. The cross talk observed between these peaks and the observed decrease peak width was indicative of the extent of Hydrogen bonding within different α,α-trehalose and their aqueous environment.

2D IR synchronous correlation analysis has proven essential to understanding the molecular events of Hydrogen bonding dynamics that occurred during all phases of crystallization of trehalose: from solution, nucleation, crystallization and crystal growth during thermal perturbation (Figs. 2 and 3). HSI's defined the events of the crystallization process and therefore the data segments used. This approach resulted in a synchronous plot comprised of the QCL IR spectral data set defined as pre-transition phase from 24 - 36 ºC (Fig. 2A) and the associated HSI representative of a homogeneous solution. The auto peaks can be defined as two subsets: 1760 – 1450 cm^{-1} as peaks associated with H_2O, while the spectral region comprised of 1450 - 1200 cm^{-1} are peaks associated with trehalose. In general, the width of these peaks (auto and cross peaks) are large when compared to the synchronous plots at higher temperature ranges (Fig. 2B and C), suggesting the extent of Hydrogen bonding α,α-trehalose has with water is high. Dramatic changes are observed within both the HSI and the synchronous plot within the temperature range of 40 - 44 ºC referred to as the nucleation to crystallization phase (Fig. 2B). The concentric circle

observed in the HSI at 40 °C due to liquid-liquid phase separation or nucleation, while the HSI at 44 °C contains a trehalose crystal. The synchronous plot dramatically changed when compared to the pre-transition synchronous plot. The auto peaks can be defined into several subsets and the largest intensity change auto peak is due to H_2O bending vibration (1651 cm^{-1}), suggesting rearrangement of H_2O molecules and the onset of the dehydration of trehalose. During crystal growth phase within the temperature range of 52 - 60 °C (Fig. 2C) the HSI contains an α,α-trehalose crystal and the synchronous plot is comprised of both auto and cross peaks that have dramatically smaller peak widths, suggesting that trehalose is primarily Hydrogen bonding between trehaloses and, to a lesser extent, with H_2O. The bulk water Hydrogen bonding dynamics are no longer a factor.

Detailed examination of the QCL IR spectral overlay and associated synchronous plots within the spectral region of 1760 - 1200 cm^{-1} provides an understanding of the intermolecular Hydrogen bonding interactions and the flexibility of the trehalose (Fig. 3A-C and Table 1). The overall intensity changes can be observed for each QCL IR spectra within the ROI due to the crystallization process under thermal stress (Fig. 3A-C). ***Pre-transition phase*** synchronous contained auto peaks 1683, 1638 and 1613 cm^{-1} are all associated with H_2O bending vibrations that are affected by thermal perturbation due to weakening of the Hydrogen bonding interactions involving H_2O molecules (Fig 3D). In addition, the synchronous plot contained α,α-trehalose associated auto peaks 1416, 1320 and 1237 cm^{-1} associated with δ(O-H) for carbon 2, 3 and 6 of the first pyranose ring, respectively; suggesting the transition from anhydrous to dihydrate state while in solution during the initial thermal perturbation. These auto peaks also had cross peaks that correlated with all of the auto peaks, suggesting the trehalose was interacting via Hydrogen bonding with other trehalose molecules and H_2O within the temperature range of 24-36 °C (Fig 3D). However, during the ***nucleation and crystallization phase transition*** the synchronous plot changes dramatically containing only one main auto peak at 1651 cm^{-1} due to H_2O bending vibrational mode ($\delta(H_2O)$), suggesting decreased variability in the types of Hydrogen bonding events. Also included, are several auto peaks associated with trehalose δ(O-H) at 1435, 1422, 1377, 1314, 1256, and 1231 cm^{-1} involving both pyranose rings with the corresponding cross peaks. Correlations between the δ(O-H) 1435 and 1231 cm^{-1} suggest intermolecular Hydrogen bonding between trehalose molecules, Also, the main auto peak associated with water $\delta(H_2O)$ at 1651 cm^{-1}, suggests that the main molecular event is due to the aqueous environment of trehalose. Where H_2O is behaving as bulk water and no longer contributing to the immediate surroundings of trehalose to allow for Hydrogen bonding interaction between the two types of molecules (Fig 3E). For the ***crystal growth phase***, a more detailed synchronous plot is observed with both the auto and cross peaks having decreased peak width suggesting less Hydrogen bonding interactions (Fig 3F). The synchronous plot for the temperature range 52 - 60 °C contains three main auto peaks: two H_2O bending vibrations (1643 and 1631 cm^{-1}) associated with bulk water and the dihydrate within trehalose, respectively; the third auto peaks 1453 and 1443 cm^{-1} associated with both rings carbon 6 and 6' $\delta(CH_2)$ due to the thermal perturbation of the α,α-trehalose. Finally, the bending vibrations δ(O-H) 1458, 1332 and 1274 cm^{-1} for carbons 4, 3 and 6 associated with the first pyranose ring are correlated to each other. Similarly, the bending vibrations δ(O-H) 1312, 11236 and 1250 cm^{-1} for carbons 4', 3' and 6' within the second pyranose ring are correlated suggesting there are intermolecular Hydrogen bonding interactions as well.

4. Conclusion

To our knowledge this is the first time a detailed molecular description of trehalose crystallization has been defined using innovative quantum cascade laser microscopy for the real-

time monitoring of the crystallization process. Moreover, the use of 2D IR correlation spectroscopy has proven to be an excellent technique to study the dynamics of Hydrogen bonding during crystallization upon thermal perturbation. This approach may be applied in the future towards the evaluation of crystallization screening efforts.

Acknowledgments

The authors would like to thank University of Puerto Rico Mayagüez Campus for granting Dr. Belinda Pastrana-Rios leave of absence without pay and the funding support of NSF SBIR Awards 14478918 and 1632420 (BPR).

Michael Meléndez: Crystallization screen and Hyperspectral Image acquisition.
Yesenia M. Acevedo Rivera: Initial spectral data analysis, writing of introduction and generation of Figures and table.
Belinda Pastrana-Rios: Conceptualization of experimental design, 2D IR correlation analysis and writing of the manuscript, reviewing and editing.

At the time of experimental runs associated with the crystallization of α,α-Trehalose, Protein Dynamic Solutions, Inc. was located in PR. Currently, Yesenia M. Acevedo Rivera is a graduate student at the University of Puerto Rico Medical Sciences, Biochemistry department and Michael Melendez is a scientist at CDI labs in Mayagüez, PR.

References

[1] H.J. Lee, Y.S. Yoon, S.J. Lee, Mechanism of neuroprotection by trehalose: Controversy surrounding autophagy induction, Cell Death Dis. 9 (2018). https://doi.org/10.1038/s41419-018-0749-9.
[2] A.B. Richards, S. Krakowka, L.B. Dexter, H. Schmid, A.P.M. Wolterbeek, D.H. Waalkens-Berendsen, A. Shigoyuki, M. Kurimoto, Trehalose: A review of properties, history of use and human tolerance, and results of multiple safety studies, Food Chem. Toxicol. 40 (2002) 871–898. https://doi.org/10.1016/S0278-6915(02)00011-X.
[3] E.Y. Chi, S. Krishnan, T.W. Randolph, J.F. Carpenter, Physical Stability of Proteins in Aqueous Solution: Mechanism and Driving Forces in Nonnative Protein Aggregation, Pharm. Res. 20 (2003) 1325–1336. https://doi.org/10.1023/A:1025771421906.
[4] J.K. Kaushik, R. Bhat, Why is trehalose an exceptional protein stabilizer? An analysis of the thermal stability of proteins in the presence of the compatible osmolyte trehalose, J. Biol. Chem. 278 (2003) 26458–26465. https://doi.org/10.1074/jbc.M300815200.
[5] S.K. Singh, Sucrose and Trehalose in Therapeutic Protein Formulations, Springer International Publishing, 2018. https://doi.org/10.1007/978-3-319-90603-4_3.
[6] J.F. Carpenter, S.J. Prestrelski, T. Arakawa, Separation of Freezing- and Dring-Induced Denaturation of Lyophilized Proteins Using Stress-Specific Stabilization; Arch. Biochem. and Biophys. (1993) 456–464.
[7] J.F. Carpenter, J.H. Crowe, An infrared spectroscopic study of the interactions of carbohydrates with dried proteins, Biochemistry. 28 (1989) 3916–3922. https://doi.org/10.1021/bi00435a044.
[8] A. Lerbret, P. Bordat, F. Affouard, Y. Guinet, A. Hédoux, L. Paccou, D. Prévost, M. Descamps, Influence of homologous disaccharides on the hydrogen-bond network of water: Complementary Raman scattering experiments and molecular dynamics simulations, Carbohydr. Res. 340 (2005) 881–887. https://doi.org/10.1016/j.carres.2005.01.036.

[9] S. Magazù, C. Branca, F. Migliardo, G. Romeo, A. Mangione, Scattering findings on disaccharide/water mixtures, J. Mol. Struct. 700 (2004) 211–215. https://doi.org/10.1016/j.molstruc.2004.01.049.
[10] N.W. Warne, Challenges in Product Development, 2012. https://doi.org/10.4135/9781452231402.n10.
[11] A. Lerbret, P. Bordat, F. Affouard, M. Descamps, F. Migliardo, How homogeneous are the trehalose, maltose, and sucrose water solutions? An insight from molecular dynamics simulations, J. Phys. Chem. B. 109 (2005) 11046–11057. https://doi.org/10.1021/jp0468657.
[12] A. Gharsallaoui, B. Rogé, M. Mathlouthi, Water-disaccharides interactions in saturated solution and the crystallization conditions, Food Chem. 106 (2008) 1329–1339. https://doi.org/10.1016/j.foodchem.2006.12.068.
[13] ACD/ChemSketch(Freeware). version 2017.2.1, Advanced Chemistry Development, Inc., Toronto, On, Canada, www.acdlabs.com, (2019).
[14] I. Noda, Advances in two-dimensional correlation spectroscopy, Vib. Spectrosc. 36 (2) (2004) 143-165.
[15] I. Noda, Recent advancement in the field of two-dimensional correlation spectroscopy, J. Mol. Struct. 883-884 (2008) 2-26.
[16] I. Noda, Techniques of two-dimensional (2D) correlation spectroscopy useful in life science research, Biomed. Spectrosc. Imaging. 4 (2015) 109-127.
[17] G. I. Olgenblum, L. Sapir, D. Harries, Properties of aqueous trehalose mixtures: Glass transition and hydrogen bonding, J. Chem. Theory Comput. 16 (2020) 1249 – 1262.
[18] R. Stuart Tipson, Infrared spectroscopy of carbohydrates: A review of the literature, National Bureau of Standards, Monograph 110 (1968) 1-20.
[19] M.J. Márquez, D. Romani, S. B. Díaz, S. A, Brandan, Structural and vibrational characterization of anhydrous and dihydrated species of trehalose based on FT-IR and Raman spectra and DFT calculations, J. King Saud Univ. – Science 30 (2018) 229-249. https://doi.org/10.1016/j.jksus.2017.01.009.
[20] H. Nagase, N. Ogawa, T. Endo, M.Shiro, H. Ueda, and M.Sakurai, Crystal structure of anhydrous form of trehalose: Structure of water channels of trehalose polymorphism, J. Phys. Chem. B. 112 (2008) 9105-9111. https://doi.org/10.1021/jp800936z.

Table 1. QCL IRM peak assignments for α,α-Trehalose[a,b] & water.

Position (cm^{-1})	Trehalose Ring Carbon Position	Assignment	Comment
Pre-transition Phase (T= 24 – 36 °C)			
1683, 1638, 1613	---	δ(H_2O)	variable H-bond
1416[a]	2	δ(O-H)	CHOH
1320[b]	3	δ(O-H)	CHOH
1237[b]	6	δ(O-H)	CH_2OH
Nucleation – Crystallization Phase (T= 40 – 44 °C)			
1651	---	δ(H_2O)	bulk water
1422[a]	4	δ(O-H)	CHOH group
1256[a]	3	δ(O-H)	CHOH group
1231[a]	6	δ(O-H)	CH_2OH group
1435[a]	3’	δ(O-H)	CHOH group
1377[a]	6’	δ(O-H)	CH_2OH group
1314[a]	4’	δ(O-H)	CHOH group
Crystal Growth Phase (T= 52-60 °C)			
1643, 1631	---	δ(H_2O)	bulk & dihydrate water
1458[a]	4	δ(O-H)	CHOH group
1332[a]	3	δ(O-H)	CHOH group
1274[a]	6	δ(O-H)	CH_2OH group
1453[a]	6	δ(CH_2)	CH_2OH group
1312[a]	4’	δ(O-H)	CHOH group
1236[a]	3’	δ(O-H)	CHOH group
1250[a]	6’	δ(O-H)	CH_2OH group
1443[a]	6’	δ(CH_2)	CH_2OH group

[a]anhydrous, [b]dihydrate

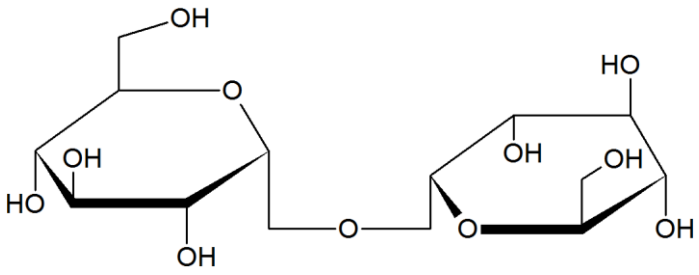

Fig. 1. Haworth diagram of α,α-Trehalose with a molecular formula of $C_{12}H_{22}O_{11}$ and molecular weight of 342.29 g/mol and for the dehydrate species the molecular weight is 378.34 g/mol [13].

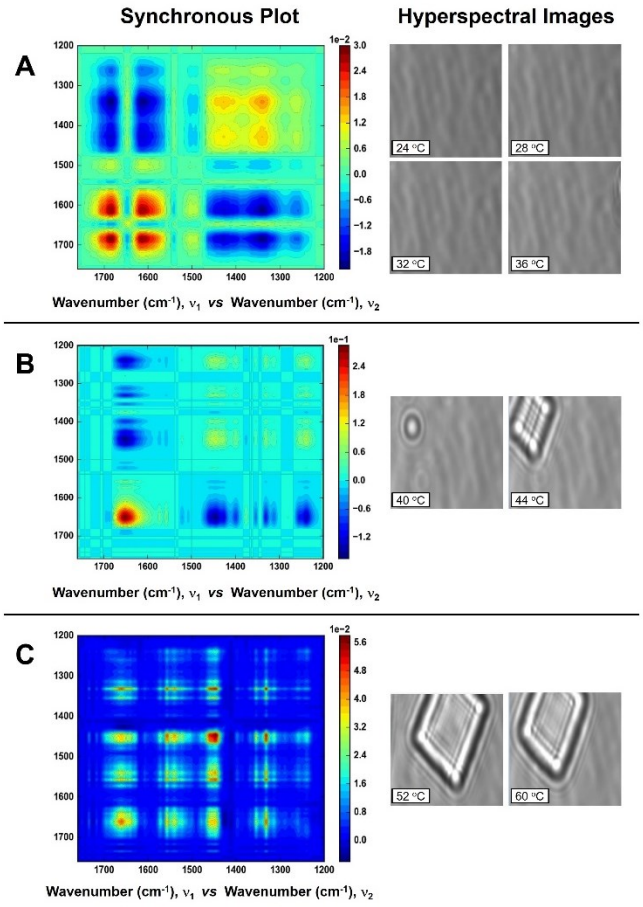

Fig. 2. Synchronous 2D IR correlation spectroscopy plot within the spectral region of 1760 -1200 cm^{-1} and hyperspectral images of solution containing 65% (w/v) α,α-Trehalose within temperature range of 24 - 60 ºC: **(A)** Temperature range 24 - 36 ºC, **(B)** Temperature range 40 - 44 ºC and **(C)** Temperature range 52 - 60 ºC.

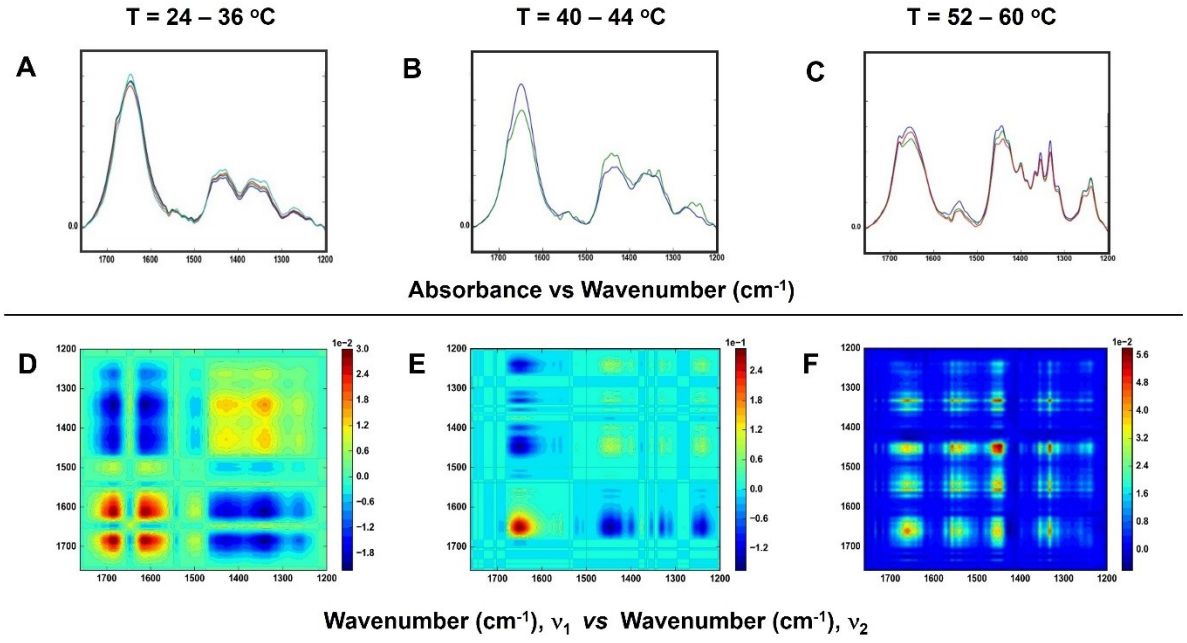

Fig. 3. Solution containing 65% (w/v) trehalose QCL IRM spectral overlay for the spectral region of 1760 - 1200 cm^{-1} within temperature range of: **(A)** 24 - 36 °C, **(B)** 40-44 °C and **(C)** 52-60 °C; and synchronous 2D IR correlation spectroscopy plots for: **(D)** the pre-transition 24 - 36 °C, **(E)** the nucleation-crystallization transition 40-44 °C and **(F)** crystal growth phase 52-60 °C.